A Generalized Strategy for 3D Dose Verification of IMRT/VMAT Using EPID-measured Transit Images

Aiping Ding, Bin Han, Lei Wang, Lei Xing

Department of Radiation Oncology, Stanford University School of Medicine, Stanford, CA 94305

Abstract
The aim in this study is to develop a generalized strategy for 3D dose verification of IMRT and VMAT planes using EPID transit images in combination with Monte Carlo (MC) simulations. An EPID-based dosimetric verification procedure was developed to convert EPID-measured transit images into 2D exit photon fluence by de-convoluting with the MC-simulated EPID response kernels. The present scatter from the phantom to the EPID was iteratively corrected by using a series of pencil beam scatter kernels derived from MC simulations. The primary fluence is therefore yielded by subtracting the corrected scatter from the total reconstructed exit fluence and used to reconstruct the dose distribution in multiple 2D planes parallel to the EPID by convoluting with the pencil beam deposition kernels. After summing up all the reconstructed 2D dose planes, the 3D dose distribution is obtained. The EPID-based dosimetric system was validated using 6 MV photon beam available from Varian TrueBeam STXTM. The results show that the EPID-based dosimetry system developed in this study is an accurate and robust tool for dose verification of IMRT/VMAT plans.

Keywords:

EPID, transit image, Monte Carlo, dose verification

1 Introduction

With more than 1.6 million new diagnoses of cancer and over one-half million projected to die of cancer in 2013, in the U.S. alone, almost 1,600 people died per day and cancer has been becoming a major health problem [1]. Radiation therapy (RT) is a major modality in cancer treatment and approximately 60% of all cancer patients in the U.S. receive RT as therapy or for palliation as an adjunct to surgery or chemotherapy. Over past two decades, intensity-modulated radiation therapy (IMRT) and volumetric-modulated arc therapy (VMAT) have become the mainstay for treating different types of cancers because of its capability of producing highly conformal dose distribution [2-9]. Practically, IMRT is composed of 5 to 10 radiation beams, with the intensity of each

adfa, p. 1, 2011.

beam modulated by a computer-controlled dynamic movement of a multi-leaf collimator (MLC). In a VMAT delivery [10-12], the position and speed of MLCs, and the gantry rotation vary dynamically [13]. While IMRT or VMAT offers a valuable tool for enhancing the therapeutic ratio and shows significant potential for improved survival and treatment outcome, their treatment planning and delivery are more technically involved and prone of errors due to dramatically increased complexity of the process. It is widely recognized that the efficacy of IMRT/VMAT can only be fully exploited with an effective quality assurance (QA) procedure to ensure the safe and efficient delivery of the exquisite dose distributions. However, current IMRT/VMAT QA procedure is labor intensive and inefficient. Moreover, it is unsafe and may lead to wrong conclusion as the measurement data are collected on one or two 2D planes, instead of 3D volume. The objective of this study is to develop a clinically practical 3D pretreatment dose verification for rapid IMRT and VMAT QA using a high spatial-resolution and high frame rate a-Si EPID and transit images in combination with Monte Carlo (MC) simulations.

2 Materials and methods

2.1 The portal electronic portal imaging device

The EPID used in this study is a standalone portable PerkinElmer XRD-0822 AP20 a-Si flat panel detector (PerkinElmer, Sunnyvale, CA). The size of detector was 20.48 × 20.48 cm^2, with a matrix of 1024 ×1024 pixels and a minimum pixel size of 0.2 mm. Its maximum frame rate is 50 frames per second (fps). The images were acquired in a "cine-mode" and a PerkinElmer image acquisition software XIS (version 3.0, PerkinElmer, Waltham, MA) was used to acquire and process all the EPID images. Measurements were performed on a Varian TrueBeam Stx Linac (Varian Medical Systems, Palo Alto, CA) for 6 MV photon beam. A source to detector distance (SDD) of 130cm and source to axis distance of 100cm were used. The thickness of the water-equivalent slab phantom was set to 20 cm and was positioned at the iso-center of the linear accelerator.

2.2 Corrections of the EPID raw images

Before images acquisition, a dark field (DF) image and a flood field (FF) image were acquired for offset and gain corrections. The offset correction took into account the dark current of each pixel and acquired with photon beam off. In order to create the offset correction image, an averaged image ($\overline{EPID}_{DF}$) of 300 frames of DF images had to be acquired and would be subtracted from the incoming pixel data during acquisition time. To homogenize differences in pixel sensitivities, an FF gain correction was carried out by irradiating the EPID with the incident photon beam fully covering the entire detector sensitive field (20×20 cm^2). To create the FF image, an averaged image ($\overline{EPID}_{FF}$) of 300 frames of offset-corrected images has to be acquired. Each EPID-measured raw image is corrected by using the following equation:

$$EPID_{raw}|_{corrected} = \frac{EPID_{raw} - \overline{EPID}_{DF}}{\overline{EPID}_{FF} - \overline{EPID}_{DF}} \quad (1)$$

2.3 EPID images to incident fluence conversion kernel

To determine the incident photon beam fluence, it was necessary to simulate and calibrate the EPID device to establish a relationship between EPID pixel values and radiation dose. Detailed structure and composition of the EPID were provided by the manufacturer and were modeled using the GATE (Geant4 Application for Tomographic Emission) [14] to generate a deconvolution kernel $K_{de}(x, y)$. The incident photon fluence $\Phi_M(x, y)$ on the EPID can thereafter be reconstructed from the corrected EPID raw image using the flowing equation:

$$\Phi_M(x, y) = (\overline{EPID}_{raw}|_{corrected}(x, y)) \otimes^{-1} (K_{de}(x, y)) \quad (2)$$

2.4 Scatter prediction kernels

When the EPID was placed close to the phantom, a large amount of scattered radiation is incident on the EPID surface. Therefore, the EPID-measured transit fluence (Φ_M) behind a slab phantom comprises primary Φ_p (un-scattered) and scattered contribution (Φ_S), that is

$$\Phi_M = \Phi_p + \Phi_S \quad (3)$$

In order to reconstruct the dose distribution with the phantom using the transmit images Φ_M, those scatter must be removed firstly.

MCNPX [15] was used to produce a series of MC scatter kernels, which allows scatter fluence predications from uniform water slab phantoms exposed to a divergent beam. It simulates a pencil beam impinging upon a slab phantom from divergent angels separately. The phantom is water-equivalent with a thickness of 20 cm. The scattered radiation present in the EPID surface was estimated point-by-point with the MC-generated pencil beam scatter kernel and was iteratively scatter-corrected using the MC simulated scatter kernels which give the primary fluence Φ_p at the plane of the EPID.

2.5 Dose deposition kernels

The extracted primary fluence at the EPID plane is scatter-corrected and converted to 2D dose distributions within the phantom in multiple planes parallel to the EPID. By summing up the 2D dose planes, the 3D dose distribution is obtained. A series of pencil-beam dose kernel $K_{pb}(x, y)$ was simulated using the MCNPX code at different depths of the slab phantoms for the dose reconstruction.

3 Results

A de-convolving dose kernel $K_{dp}(x, y)$ was generated from GATE MC simulations with the consideration of the MV photon dose deposition in the EPID screen, the optical photon creating and scattering process, as shown in Fig.1. The incident photon fluence on the EPID was therefore reconstructed from the corrected EPID raw images.

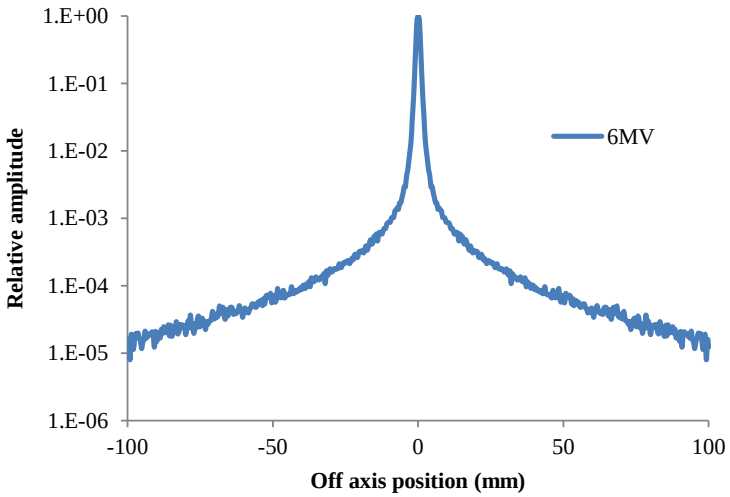

Fig. 1. The GATE generated kernel used in de-convolution of EPID-measured raw images to incident photon fluence.

Fig.2 shows an example of MCNPX simulated scatter prediction kernel. During the MC simulation, two separated tallies were simultaneously used to record the fluence from scatter only and primary plus scatter on the EPID plane.

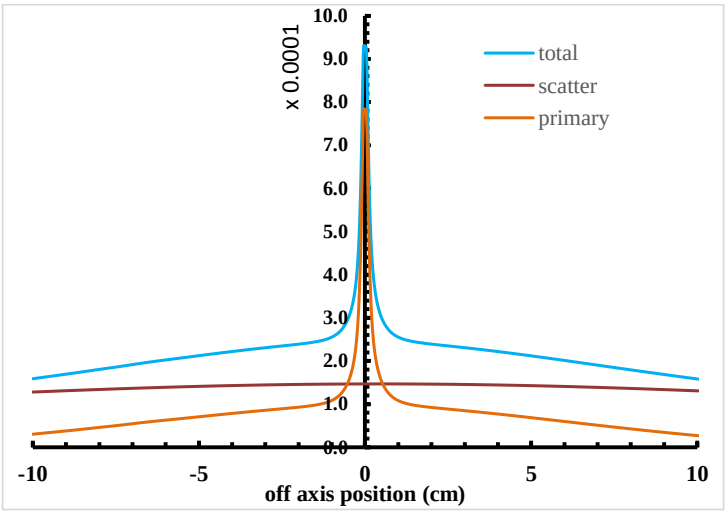

Fig. 2. An example of MCNPX simulated scatter prediction kernel used to remove the scatter from the reconstructed transit fluence.

Fig.3. shows the simulated $K_{pb}(x, y)$ of pencil beam used in the dose reconstruction.

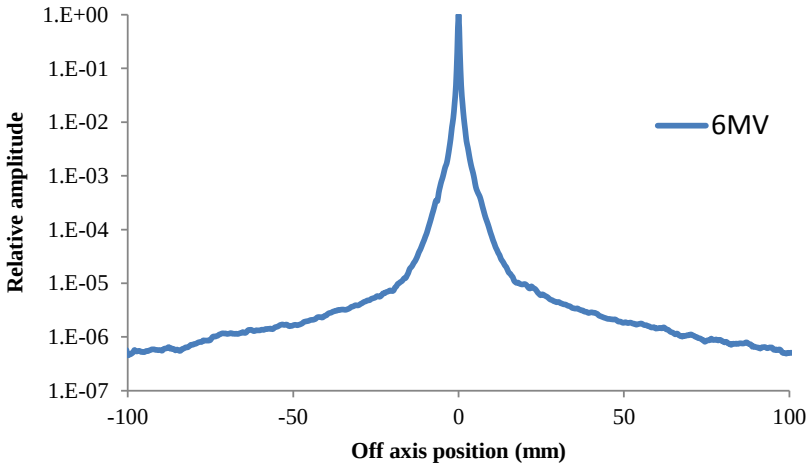

Fig. 3. The MCNPX generated dose kernel used in the dose reconstruction

To evaluate the performance EPID dosimetry system on photon beam applications, the absolute 2D dose distribution of square fields of 4×4 to 15×15 cm^2 fields were tested firstly against water scan results and PTW729 ion chamber array measurements, as shown in Fig.4.

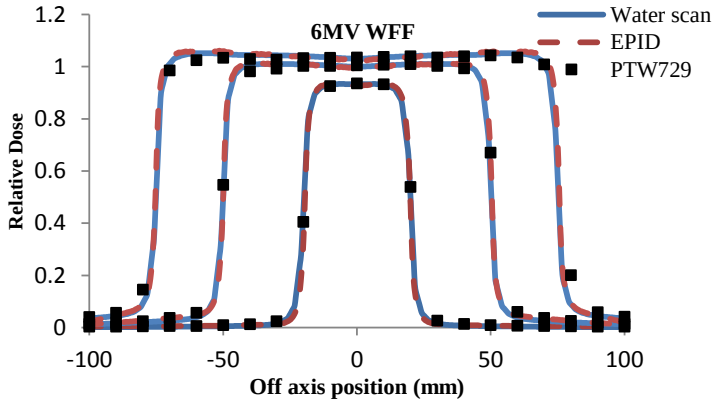

Fig. 4. Water-scan, PTW729, and EPID-measured dose profiles

To further validate the EPID measurement, one typical patient-specific case was delivered and compared with TPS calculation. Overall, as shown in Fig.5., the comparison data showed good agreement for both cases. EPID measurements vs TPS calculation, the γ-index pass rates were greater than 99% for criterion of 3%/3mm in the selected dose plane.

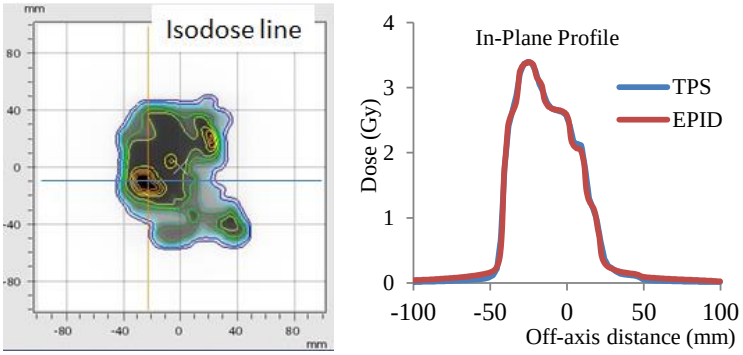

Fig. 5. Isodose line overlay of EPID measurements with TPS calculation and in-plane profiles of EPID and TPS calculation for the tested patient case.

4 Conclusions

We have developed a generalized procedure for dose verification of IMRT and VMAT using EPID transit images in combination with MC simulations. It provides a viable solution to the unmet need for a 3D dosimetric tool for IMRT/VMAT plan validation and for a number of intractable dosimetry problems, such as small fields and fields with high dose rates.

5 References

1. American Cancer Society Annual Report. http://www.cancer.org/research/cancerfactsstatistics/cancerfactsfigures2013/index (Access date: 01/13/2014).
2. Gregoire, V. and T.R. Mackie, State of the art on dose prescription, reporting and recording in Intensity-Modulated Radiation Therapy (ICRU report No. 83). Cancer Radiotherapie, 2011. 15(6-7): p. 555-559.
3. Gaspar, L.E. and M.S. Ding, A Review of Intensity-Modulated Radiation Therapy. Current Oncology Reports, 2008. 10(4): p. 294-299.
4. Sanghani, M. and J. Mignano, Intensity modulated radiation therapy: A review of current practice and future directions. Technology in Cancer Research & Treatment, 2006. 5(5): p. 447-450.
5. Nutting, C., D.P. Dearnaley, and S. Webb, Intensity modulated radiation therapy: a clinical review. British Journal of Radiology, 2000. 73(869): p. 459-469.
6. Mell, L.K., A.K. Mehrotra, and A.J. Mundt, Intensity-modulated radiation therapy use in the U.S, 2004. Cancer, 2005. 104(6): p. 1296-1303.
7. Sheets, N.C., et al., Intensity-Modulated Radiation Therapy, Proton Therapy, or Conformal Radiation Therapy and Morbidity and Disease Control in Localized Prostate Cancer. Jama-Journal of the American Medical Association, 2012. 307(15): p. 1611-1620.
8. Mell, L.K., A.K. Mehrotra, and A.J. Mundt, Intensity-modulated radiation therapy use in the U.S., 2004. Cancer, 2005. 104(6): p. 1296-1303.
9. Sheets, N.C., et al., INtensity-modulated radiation therapy, proton therapy, or conformal radiation therapy and morbidity and disease control in localized prostate cancer. JAMA, 2012. 307(15): p. 1611-1620.
10. Mackie, T.R., et al., Tomotherapy - a New Concept for the Delivery of Dynamic Conformal Radiotherapy. Medical Physics, 1993. 20(6): p. 1709-1719.
11. Yu, C.X., Intensity-Modulated Arc Therapy with Dynamic Multileaf Collimation - an Alternative to Tomotherapy. Physics in Medicine and Biology, 1995. 40(9): p. 1435-1449.
12. Otto, K., Volumetric modulated arc therapy: IMRT in a single gantry arc. Medical Physics, 2008. 35(1): p. 310-317.
13. Wolff, D., et al., Volumetric modulated arc therapy (VMAT) vs. serial tomotherapy, step-and-shoot IMRT and 3D-conformal RT for treatment of prostate cancer. Radiotherapy and Oncology, 2009. 93(2): p. 226-233.
14. Jan S et al 2010 GATE V6: a major enhancement of the GATE simulation platform enabling modelling of CT and radiotherapy Phys. Med. Biol. 56 881-901
15. D.B. Pelowitz, MCNPX USER'S MANUAL. (Los Alamos National Laboratory, Los Alamos, NM, 2005).